Raman Scattering Studies of the Ba_2MnWO_6 and Sr_2MnWO_6 Double Perovskites

Yukari Fujioka,*,†,‡ Johannes Frantti,†,‡ and Masato Kakihana†,§

Materials and Structures Laboratory, Tokyo Institute of Technology, 4259 Nagatsuta, Midori-ku, Yokohama 226-8503, Japan, and Institute of Multidisciplinary Research for Advanced Materials, Tohoku University, Sendai 980-8577, Japan

Received: August 28, 2005; In Final Form: November 14, 2005

Polycrystalline Ba_2MnWO_6 (BMW) and Sr_2MnWO_6 (SMW) samples were studied between 80 and 1200 K by Raman scattering spectroscopy. In the case of BMW (space group $Fm\bar{3}m$), four Raman active vibrational modes, predicted by factor group analysis, were identified. Raman scattering studies with different wavelengths revealed a resonant bands between 300 and 800 cm^{-1}. The origin of these bands was related to the Franck−Condon process. Line broadening versus temperature and phonon frequency were studied, and a qualitative explanation was proposed. SMW samples had considerably more complex Raman spectra. It was found that SMW transformed from tetragonal (room-temperature space group $P4_2/n$) to the cubic phase between 670 and 690 K; the phase transition temperature was dependent on sample preparation conditions, and it was considerably lower than in the case of large grain size powders. The role of grain size in phase transition is discussed. Mn ions were found to have a crucial role in the lattice dynamics of both materials.

1. Introduction

Despite their simple crystal structure, perovskites show a rich variety of technologically important properties, such as superconductivity, ferroelectricity, and numerous magnetic phenomena. In many occasions, perovskites are modified by substituting A- and/or B-cations by other atoms. From the structural point of view, the resulting materials can broadly be divided into two classes: disordered and ordered. The first category includes materials where the substituted site is statistically occupied by different atoms, as is the case of lead zirconate titanate (PZT).[1] In the second category, there is a precisely determined order among the cations, as is found from $(NH_4)_3FeF_6$.[2] When the B-site atoms array alternatively in three directions, it has been customary to call these perovskite materials "double perovskites".

In some cases, ordering crucially affects physical properties. For instance, Sr_2FeMoO_6 (SFM), which is anticipated to be a room-temperature colossal magnetoresistance (CMR) material, has been reported to have various degrees of ordering.[3] In the case of SFM, the higher the degree of ordering is, the greater the CMR effect generated. As the degree of cation ordering correlates with the physical properties, it is of crucial importance to quantify it experimentally. Diffraction techniques are not always well suited for the estimation of the degree of ordering, except the two extreme cases of "perfect order" and "complete disorder". Even in the case of perfect order, the superstructure Bragg reflections are typically weak. In contrast, the number of Raman active modes is dominated by the site symmetries of the ions. Raman scattering is sensitive to deviations from the ideal symmetry, such as those due to the mixing of B-cations. Therefore, it is easier to estimate the cation ordering by Raman spectroscopy. The ideal double perovskite with space group $Fm\bar{3}m$ and one formula unit per primitive cell has four Raman active modes, in contrast to the case of a disordered perovskite with space group $Pm\bar{3}m$ with no Raman active mode. Our first aim was to study optical phonons of two A_2MnWO_6 (A = Ba, Sr) perovskites by Raman spectroscopy. Mn and W ions are likely to be ordered due to the large differences in valence and ionic radii: the ionic radius of Mn^{2+} is 0.97 Å, and that of W^{6+} is 0.74 Å.[4] Ba_2MnWO_6 (BMW) with the large Ba ion is cubic, while the room-temperature structure of Sr_2MnWO_6 (SMW) is often distorted from the cubic symmetry due to the smaller ionic radius of the Sr ion, although the crystal symmetry depends as well on the exact stoichiometry of the samples. Thus, Raman spectroscopy was used to confirm the previous space group symmetry assignments given for BMW and SMW samples by studying the number of Raman active modes and the line widths. This is closely related to the estimation of the B-cation ordering. The idea is to study if the given space group assignments are consistent with the Raman scattering data. Raman spectroscopy is also sensitive to the vibrations involving light elements, such as oxygen. This in turn allows oxygen octahedra modes to be studied. Particular attention was paid to the temperature dependence of the Raman peak widths of different modes. Our second goal was to study the role of Mn ions in the lattice dynamics by exciting Raman spectra using different wavelengths. The role of Mn ions, through their valence, is crucial for the crystal symmetry, magnetic ordering, and magnetic moment. As a third topic, possible symmetry changes occurring as a function of temperature were studied. The common starting point for all cases is the symmetry analysis, which is based on previous X-ray and neutron powder diffraction studies and given prior to the experimental data.

2. Experimental Section

2.1. Sample Preparation. Polycrystalline BMW and SMW samples were prepared by the polymerizable complex (PC) method. The PC method is known as a superior technique for

* To whom correspondence should be addressed. E-mail: yfu@fyslab.hut.fi.

† Tokyo Institute of Technology.

‡ Present address: Laboratory of Physics, Helsinki University of Technology, P.O. Box 1100, FIN-02015 HUT, Finland.

§ Tohoku University.

10.1021/jp054861b CCC: $33.50
Published on Web 12/21/2005

the synthesis of crystalline powders.[5] Ester reactions between citric acid (CA) and ethylene glycol (EG) result in polyester resin. This step is of central importance for the synthesis of highly homogeneous powders at comparatively low temperatures.

While synthesizing BMW and SMW samples, the AWO_4 scheelite structure impurity phase is easily formed.[8] Therefore, Ba (or other alkali earth elements) ions and W ions should be preserved from conjunction with each other. In the PC method, cations are "frozen" into polymer networks and do not easily diffuse because of their low mobility. Once pyrolysis of polymer resin occurs, cations diffuse and form the compound. In the case of the PC method, required diffusion distances are short, which makes low-temperature synthesis possible.

The excess of CA over the total mole number of cations was dissolved into aqueous EG solution with molar ratio of CA:EG = 1/4, and $BaCO_3$ or $SrCO_3$, MnO, and W-peroxo solution were added into the citric solution. The resultant transparent and yellowish solution was heated to around 400 K over several hours to promote esterification between CA and EG, and it gelled into a brown glassy resin. Charring this resin up to 720 K resulted in a black powder. This black powder was calcined at 873 K for 12 h in a vacuum furnace. Calcined powder was ground and pressed into pellets. They were annealed at 1273 K for 12 h (for BMW) or 1073 K for 12 or 24 h (for SMW) in an encapsulated quartz tube containing Ta foil to absorb the possible residual oxygen inside the tube. Further details including characterizations of BMW and SMW powders are also given in refs 6 and 7.

2.2. Raman Measurements. Raman measurements were performed using a Jobin-Yvon T64000 spectrometer consisting of a double monochromator coupled to the third monochromator stage with 1800 grooves per millimeter grating (double substractive mode). Prior to measurements, the spectrometer was calibrated with an Ne lamp.

The acquisition time was adjusted to have a sufficient signal-to-noise ratio. A charge-coupled device detector was used to count photons. All measurements were carried out under the microscope in a backscattering configuration. Raman spectra were excited using an Ar^+/Kr^+ laser (Spectra Physics) and a He−Ne laser (Melles Griot). The laser beam power on the sample surface was 100 μW, and the diameter of the laser beam spot was approximately 2 μm. It was essential to keep the laser beam power sufficiently low as BMW and SMW samples are easily decomposed due to the laser beam irradiation. Decomposition was revealed by the additional peaks appearing at high laser beam powers. The exact decomposition mechanism was not identified, but the use of an inert gas atmosphere (N_2 or Ar) together with a small laser beam power density was found to be sufficient to prevent the decomposition. Modest laser beam power also ensured that the local heating during low-temperature measurements was neglible. Linkam chamber (model TS-1500 and THMS-600) and temperature controlling unit (model LK-600PH) were used for the room-, high-, and low-temperature measurements.

Raman spectra were analyzed using commercial curve fit software, Jandel Scientific PeakFit 4.0.

3. Symmetry Assignment of Raman Active Modes

Table 1 specifies the room-temperature structures (space groups and site symmetries of ions were adapted from refs 8 and 9 (BMW) and 10 (SMW)) and the corresponding normal modes of vibrations at the Brillouin zone center of the BMW and SMW double perovskites. As the symmetry of the BMW crystal is high, one can make the following assignments: the highest frequency mode is the A_{1g} mode, and the two lowest frequency modes are the T_{2g} modes. The assignment is based on the following reasoning: the A_{1g} and E_g modes involve only oxygen motion, while the T_{2g} modes involve additionally Ba ions, as indicated in Table 1. Further, in the A_{1g} mode, all oxygen ions move toward (outward) the oxygen octahedra center, while in the case of the E_g mode four coplanar oxygen ions move toward (outward) the octahedra center and the other two oxygen ions move outward (toward) the center. Correspondingly, the A_{1g} mode has a stiffer force constant than the E_g mode. Usually, the totally symmetric modes have the strongest intensities. Thus, one expects the A_{1g} peak to have higher intensity than the other modes. Similar conclusions were drawn in ref 11, where several cubic double perovskites were studied. In ref 11, the E_g mode was reported to usually be very weak.

TABLE 1: Structure and the Irreducible Representations of the Normal Modes of Vibrations at the Brillouin Zone Center k = 0 Corresponding to the BMW and SMW Samples[a]

atom	wyckoff position	fractional coordinates	site symmetry	irreducible representations
Space Group: $Fm\bar{3}m$ (No. 225)				
Ba	8*c*	($^1/_4$ $^1/_4$ $^1/_4$)	$4\bar{3}m$	T_{1u}, T_{2g}
Mn	4*a*	(000)	$m\bar{3}m$	T_{1u}
W	4*b*	($^1/_2$ $^1/_2$ $^1/_2$)	$m\bar{3}m$	T_{1u}
O	24*e*	(*x*00)	4*mm*	A_{1g}, E_g, T_{1g}, $2T_{1u}$, T_{2g}, T_{2u}
$\Gamma_R = A_{1g} \oplus E_g \oplus 2T_{2g}$				
$\Gamma_{IR} = 4T_{1u}$				
$\Gamma_S = T_{1g} \oplus T_{2u}$				
$\Gamma_A = T_{1u}$				
Space Group: $P4_2/n$ (No. 86)				
Sr(1)	2*a*	($^1/_4$ $^1/_4$ $^1/_4$)	$\bar{4}$	B_g, E_g, A_u, E_u
Sr(2)	2*a*	($^1/_4$ $^1/_4$ $^1/_4$)	$\bar{4}$	B_g, E_g, A_u, E_u
Sr(3)	4*e*	($^3/_4$ $^1/_4$ *z*)	2	A_g, B_g, $2E_g$, A_u, B_u, $2E_u$
Mn	4*c*	(000)	$\bar{1}$	$3A_u$, $3B_u$, $3E_u$
W	4*d*	(00 $^1/_2$)	$\bar{1}$	$3A_u$, $3B_u$, $3E_u$
O(1)	8*g*	(x_1 y_1 z_1)	1	$3A_g$, $3B_g$, $3E_g$, $3A_u$, $3B_u$, $3E_u$
O(2)	8*g*	(x_2 y_2 z_2)	1	$3A_g$, $3B_g$, $3E_g$, $3A_u$, $3B_u$, $3E_u$
O(3)	8*g*	(x_3 y_3 z_3)	1	$3A_g$, $3B_g$, $3E_g$, $3A_u$, $3B_u$, $3E_u$
$\Gamma_R = 10A_g \oplus 12B_g \oplus 13E_g$				
$\Gamma_{IR} = 17A_u \oplus 18E_u$				
$\Gamma_S = 16B_u$				
$\Gamma_A = A_u \oplus E_u$				

[a] Raman active, infrared active, silent, and acoustical modes are represented by the symbols Γ_R, Γ_{IR}, Γ_S, and Γ_A, respectively.

The symmetry of the SMW sample was low, resulting in a large number of Raman active modes, 35 (see Table 1). As the samples were polycrystalline, a similar line assignment to that done for BMW was not possible.

4. Results and Discussion

4.1. First-Order Raman Spectra. 4.1.1. Ba_2MnWO_6 Samples. Figure 1 shows the laser beam wavelength (λ) dependence of the room-temperature Raman spectra of BMW powders. As predicted by the symmetry analysis, four phonon peaks were observed in the spectra excited by $\lambda = 476.5$ nm and $\lambda = 514.5$ nm light. The symmetry assignment of the peaks was based on the reasoning given above.

In addition to the four identified peaks, several weak peaks are shown in the spectrum excited by $\lambda = 632.8$ nm in Figure 1 between 450 and 750 cm^{-1}. Figure 2 shows Stokes and anti-Stokes Raman spectra using $\lambda = 647.1$ nm, in which these weak modes were observed in both spectra. The intensity of these peaks was decreasing with increasing temperature and decreasing λ. Most of these peaks appeared equidistantly. This type of

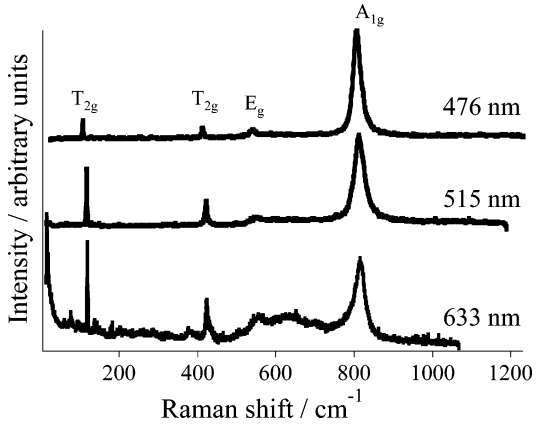

Figure 1. Raman spectra collected from the BMW sample (sintered at 1273 K) using various excitation wavelengths. The intensities were scaled by a constant in a way that the peaks at around 830 cm^{-1} had equal intensities to allow an easy comparison. Due to the resonance, the symmetry assignments are not strictly valid for the spectrum excited by a 633 nm wavelength light.

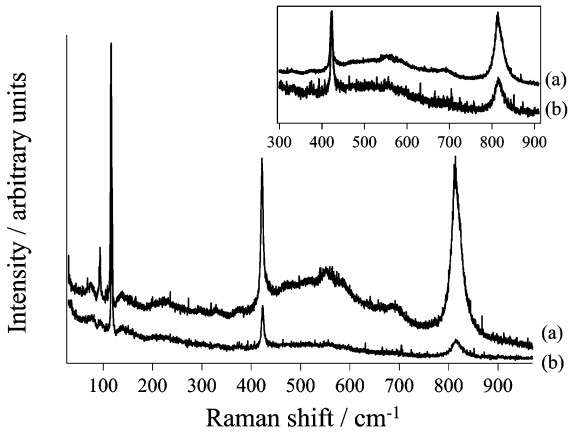

Figure 2. Stokes (a) and anti-Stokes (b) Raman spectra collected from the BMW sample at room temperature (λ = 647.1 nm). Vertically enlarged spectra are shown in the small panel (the intensity of the anti-Stokes spectrum was multiplied by a factor of 5). Franck−Condon overtone modes are seen in the region between 450 and 750 cm^{-1} on both Stokes and anti-Stokes spectra.

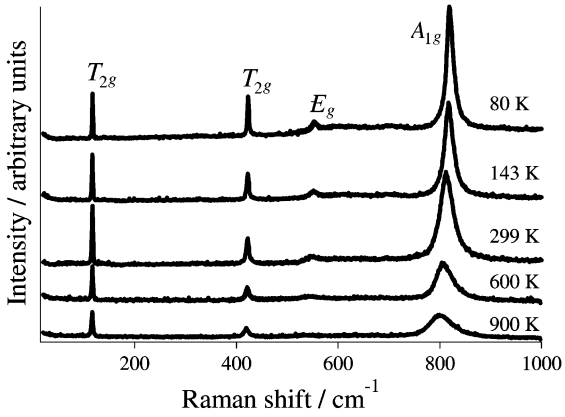

Figure 3. Raman spectra collected from the BMW sample (sintered at 1273 K) at various temperatures (λ = 515 nm). Labeling of the peaks was based on the symmetry analysis, see text for details.

resonance phenomena relies on real electronic transitions. The consequence is that not only are the intensities of first-order Raman modes affected but also often new, informative modes are created, and both the changes in first-order Raman spectra and the new modes are analyzed together to get a consistent model.

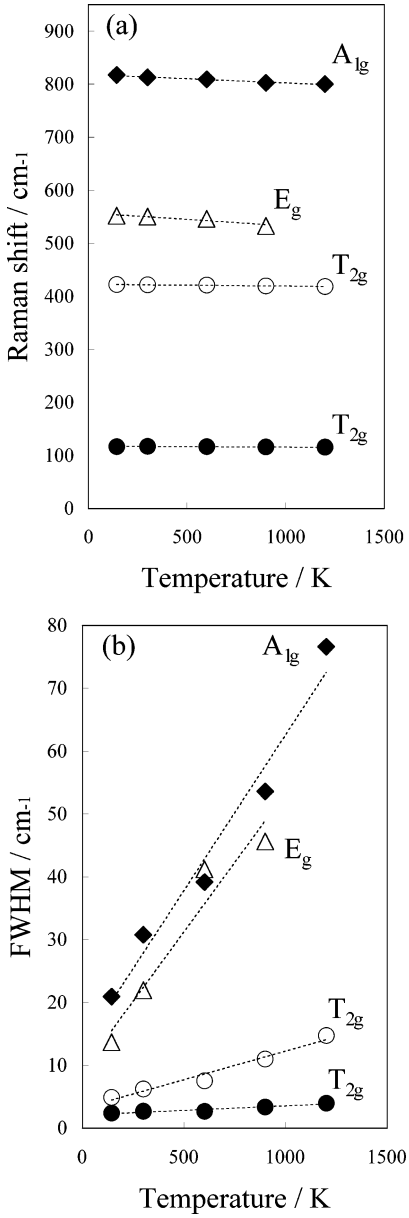

Figure 4. (a) Positions of the four Raman peaks of the BMW sample (sintered at 1273 K) and (b) fwhm values of the T_{2g}, E_g, and A_{1g} symmetry modes. In the case of the A_{1g} modes, peaks were fitted using the asymmetrical Pearson IV function, while the other peaks were modeled by the pseudo-Voigt function. In both panels, the broken lines are guides for the eyes.

Similar features were observed in a cubic SMW single crystal for which polarization Raman scattering experiments were carried out.[12] By studying the frequency, symmetry, intensity, λ, and temperature dependence of the modes, we could model and assign the origin of the peaks from the point of view of the Franck−Condon principle.[12] The electronic transition was related to the e_g to e_g transition at Mn ions. Also, the decrease of the A_{1g} mode intensity with increasing λ (Figure 1) is consistent with this observation: due to the Mn ion shift, the oxygen octahedra is distorted and the vibration is no longer totally symmetric. This was most clearly seen from the intensity ratio between the A_{1g} and T_{2g} modes at around 420 cm^{-1}: the ratio decreases with increasing λ. This feature also shows that Mn ions significantly contribute to the lattice dynamics of these materials, in contrast to the proposal given in ref 11, where the role of W was considered as dominating. Particularly important is to know the location of Mn d-orbital states. Ab initio

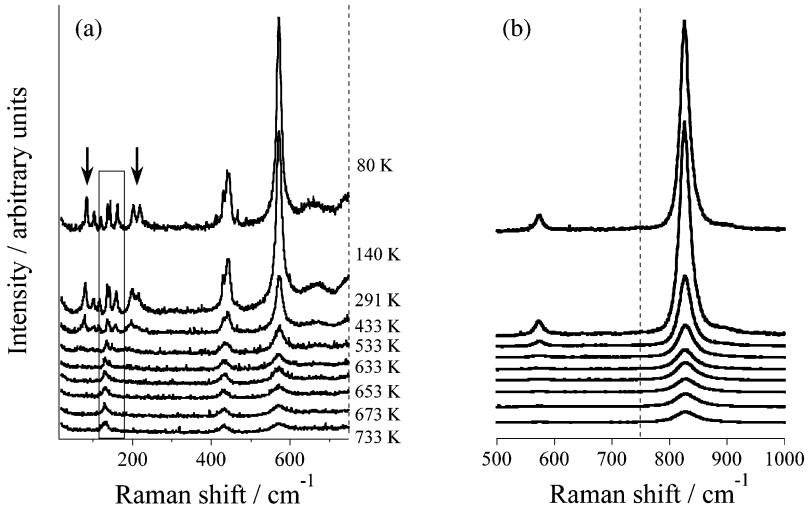

Figure 5. Raman spectra collected from the SMW sample at various temperatures ($\lambda = 515$ nm). The figure is separated into two parts in order to enlarge the spectra in the low-frequency region. The dashed line in part b indicates the right edge of part a.

computations of the electronic energy bands in these two double perovskites are in progress. It is worth noting that neutron powder diffraction (NPD) measurements indicated that the sample contained only the perovskite phase (all reflections were indexed assuming the $Fm\bar{3}m$ space group). Reference 7 gives the NPD results.

Figure 3 shows the Raman spectra collected from the BMW sample at several temperatures using an excitation wavelength of 514.5 nm. These spectra are consistent with the fact that there is a well defined order among the B-cation sites, as the previous neutron powder diffraction experiments revealed from two different samples prepared by the PC method[7] and the conventional solid-state reaction technique.[9] In the other extreme, the B-cation sites would be randomly occupied by the W and Mn ions, which would correspond to the average $Pm\bar{3}m$ space group with no Raman active modes. However, most of the cases fall between these two extremes, and the full-width-at-half-maximum (fwhm) values of Raman peaks depend also on the ordering at the B-cation sites. We did not see any evidence for the symmetry lowering, and the Raman spectra at the temperature range studied were consistent with the space group $Fm\bar{3}m$.

Peak positions and fwhm values of the BMW samples are shown in Figure 4. It is seen that the two T_{2g} modes were rather narrow, when compared to the oxygen octahedra modes. The fwhm values of the A_{1g} and E_g modes were strongly dependent on temperature. As Figure 4b demonstrates, the higher the frequency of the normal mode, the larger the fwhm value. In the case of the four identified phonon peaks, it is seen from Figure 4b that the fwhm value of the highest frequency mode (A_{1g} symmetry) is most susceptible to temperature, while the lowest frequency mode has an almost constant fwhm value. These two features can qualitatively be understood by considering the dependence of the vibration amplitude on the temperature and frequency. As is shown in ref 13, one can derive an equation $\langle|Q(\mathbf{k},\nu)|^2\rangle = \hbar/\omega(\mathbf{k},\nu)(n(\omega,T) + {}^1/_2)$ for the normal mode amplitude $Q(\mathbf{k},\nu)$, where $\mathbf{k}$ is the wave vector, ν labels the phonon branch, ω is the angular frequency, T is temperature, and n is the Bose−Einstein distribution function. Thus, once the frequency (or temperature) is increasing, the mean square value of the normal mode amplitude increases. As the amplitude increases, the contribution from the anharmonic interactions becomes more significant, which results in the observed line broadening phenomenon. Intuitively, this is plausible, as the two highest frequency modes involve only oxygen ions, which undergo long excursions from their equilibrium positions, while the two lowest frequency modes also involve heavy Ba ions, in addition to the oxygen ions. Thus, the observed line broadening does not seem to correspond to the mixing of Mn and W sites, as is demonstrated by the very small fwhm values of the T_{2g} modes. We note that even though the T_{2g} modes involve only oxygen and Ba (see Table 1), their narrow fwhm values are consistent with the idea that there is hardly any mixing of Mn and W. To see this, we note that in a case of significant mixing the symmetry is essentially lost and the normal mode basis function assignment, given in Table 1, is no longer valid. A well known example is PZT, whose high-temperature Raman spectra, consisting of broad and relatively strong bands, do not correspond to the $Pm\bar{3}m$ symmetry, even though the diffraction pattern is well indexed by assuming a prototype perovskite structure. Also, the fact that the asymmetry of the line shape of the A_{1g} peak was increasing with increasing temperature supports the idea that the anharmonic interactions are prominent for this mode.

4.1.2. Sr_2MnWO_6 Samples. Figure 5 shows selected Raman spectra collected from the SMW sample at various temperatures. Positions and fwhm values of selected Raman peaks are shown in Figure 6. We note that similar resonance modes which were found from the cubic SMW single crystal (assigned to Franck−Condon modes in ref 12) and from the cubic BMW powders in this study were also found from tetragonal SMW powders once λ was 633 nm.

Although the symmetry analysis (see Table 1) predicts 35 Raman active modes, a lesser number of separate peaks were seen. This was apparently due to the small distortions from the cubic symmetry, which resulted in overlapping peaks. Correspondingly, the oxygen vibration modes (Strictly speaking, there are no pure oxygen vibrations in the tetragonally distorted SMW. However, the distortions are so small that one can still classify the modes at 570 and 830 cm^{-1} as oxygen vibration modes.) were very similar to the corresponding modes of the BMW sample. Also, the behavior of the fwhm values was reminiscent of the case of BMW. The oxygen vibrations at around 570 and 830 cm^{-1} had the largest fwhm values, while the vibrations involving Sr had narrower line widths. The scatter in the fwhm values of the peak at around 140 cm^{-1} increases at around 600 K and reflects the fact that peak fit was somewhat ambiguous at this temperature. We related this phenomenon to the phase transition (discussed below), which obscured peak

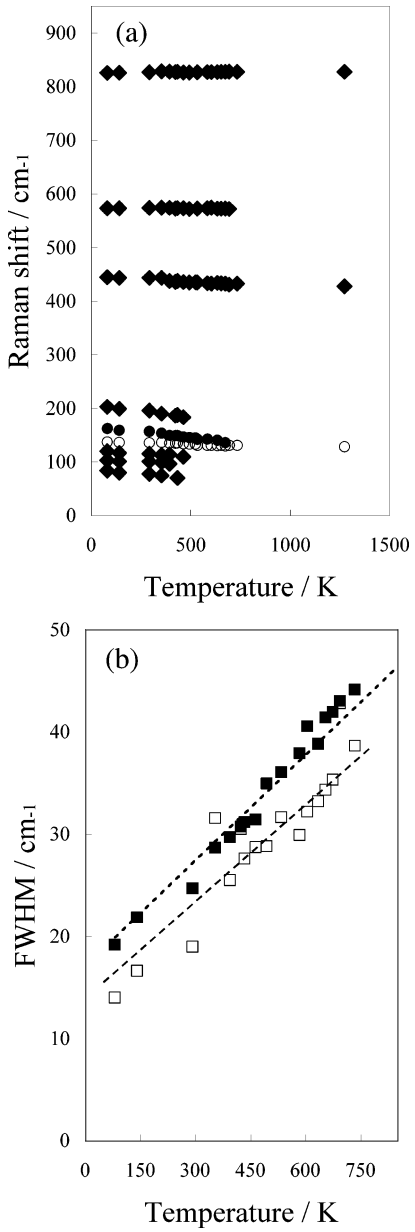

Figure 6. (a) Positions and (b) fwhm values of the selected Raman peaks of the SMW sample. The difference in Raman shift between two peaks indicated by filled and open circles in part a versus temperature is shown in Figure 8. In part b, the modes at 570 and 830 cm^{-1} are labeled by open and filled squares, respectively. The broken lines are guides for the eyes.

fit. However, as Figure 5 indicates, no soft mode behavior is seen in the Raman spectra. Thus, we studied the overall spectral changes taking place with increasing temperature. The most drastic differences between the spectra measured from the SMW and BMW samples were seen in the low-frequency region, where the peaks are significantly weaker than the T_{2g} modes of the BMW sample. In addition, many peaks were split (for instance, the doublet at around 150 cm^{-1}, shown in a frame in Figure 5) or at least significantly broader than the low-frequency peaks of the BMW sample. All peaks below the 300 cm^{-1} region, except the one at around 150 cm^{-1}, were essentially vanished at 600 K, and the spectra became reminiscent of that of the BMW sample above 700 K, indicating that the symmetry was increased to the cubic one.

To make a qualitative estimation of the phase transition temperature, we plotted the differences between the frequencies of the two peaks, $\Delta\omega$, at around 138 and 154 cm^{-1} versus temperature in Figure 8. Figure 8 shows that $\Delta\omega$ decreases with increasing temperature so that at around 693 K it became zero, and thus, it was estimated that the phase transition occurred at this temperature. An expression $\Delta\omega = \alpha(T_0 - T)^{\beta}$ was fit to these data, and the fitting resulted in values $\alpha = 1.2(3)$, $T_0 = 693(3)$ K, and $\beta = 0.47(4)$. For a comparison, a similar fitting was done for data collected on the SMW sample sintered at 1073 K for 12 h. The fit resulted in parameter values $\alpha = 1.0(3)$, $T_0 = 673(2)$ K, and $\beta = 0.49(5)$. Although not too much significance can be put on the parameters α and β, the transition temperature estimates are reasonable. We note that the difference between the peak frequencies can be fit more accurately than the individual frequencies. Figure 7 shows that at the presumed cubic phase the position of the peak at around 135 cm^{-1} was decreasing and the fwhm and intergated area were increasing with increasing temperature.

The difference between the phase transition temperatures of the two SMW samples deserves attention. Figure 8 reveals that the $\Delta\omega$ values were almost the same for both SMW samples. The main difference was that the SMW sample sintered at 1073 K had a lower transition temperature. The phase transition temperature in turn is dependent on the magnitude of the tetragonal distortion. Our neutron powder diffraction results indicated slightly larger room-temperature lattice constants and a tetragonal c/a axis ratio for the sample sintered at 1273 K ($a = 8.0187$ Å, $c = 8.0206$ Å, and $c/a \approx 1.0002$) than for the samples sintered at 1073 K ($a = 8.0157$ Å, $c = 8.0152$ Å, and $c/a \approx 0.9999$). Tetragonal distortion is affected by two factors. First, the sample stoichiometry is well known to have an impact on the symmetry and magnetic ordering in Mn containing perovskites, such as $LaMnO_3$.[14] This is mainly related to the Mn ion valence. One could anticipate that the tetragonal distortion increases with increasing Mn^{3+} ion concentration: in contrast to the Mn^{2+} ions, Mn^{3+} ions are Jahn−Teller active. The previous bond valence sum calculation for the NPD data revealed that estimated Mn valences were 2.32 and 2.35 for SMW samples sintered at 1073 and 1273 K, respectively. So far, there is no evidence that tetragonal distortion occurred due to the nonstoichiometry of the sample. The second factor is the crystal size effect. Surface energy is known to have an effect on crystal lattice distortion, which in turn affects the phase transition temperature. In addition to the effect on crystal lattice distortion and phase transition temperature, crystal size has been reported to have an influence on magnetic ordering via the crystal lattice in manganese perovskites, examples being $La_{1-x}Sr_xMnO_3$[15] and $La_{1-x}Ca_xMnO_3$[16] powders. The crystal sizes within the SMW samples sintered at 1073 and 1273 K were estimated to be 88 and 192 nm, respectively.[7] A recent neutron powder diffraction study revealed that the SMW sample, prepared through the solid-state reaction technique, transformed via an intermediate phase (the space group was $I4/m$ at 773 K) to the cubic phase (the space group was $Fm\bar{3}m$ at 973 K).[17] Thus, the phase transition was significantly higher than that observed in the present study. The room-temperature lattice parameter values were $a = 8.0119$ Å and $c = 8.0141$ Å, and the c/a ratio of this sample was 1.0003, which is very close to the value found from the present samples.[17] However, the crystal size in our powders was more than an order of magnitude smaller. We believe that it is the large surface area per volume which favors the cubic phase. Thus, it seems to be that the crystal size is the dominating factor affecting the phase transition temperature in these powders.

On heating, some Raman peaks in the low freqency region (indicated with arrows in Figure 5) vanished before the

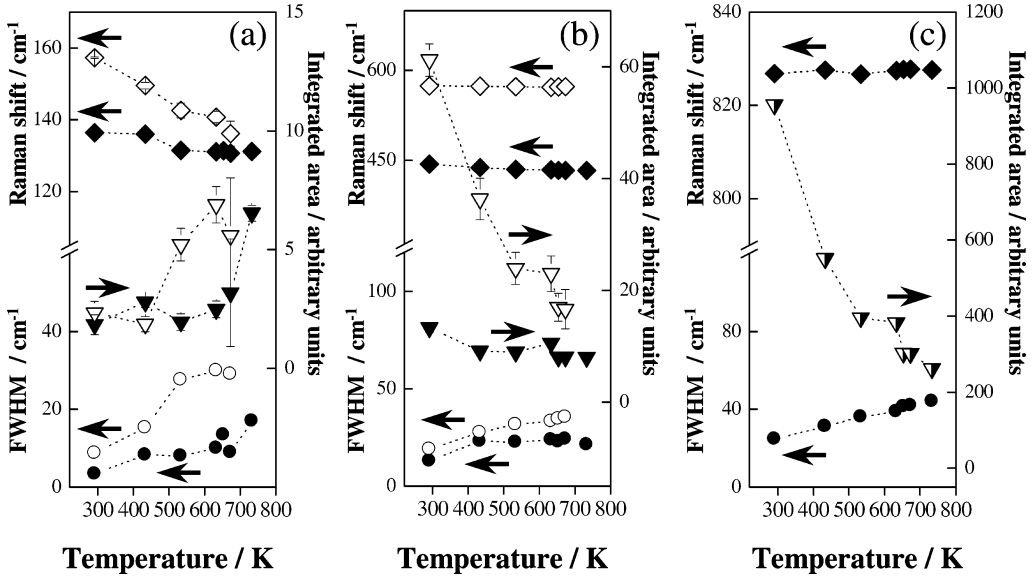

Figure 7. Positions, fwhm values, and integrated areas of selected Raman peaks measured from the SMW sample. (a) Data extracted from the two peaks shown in frame in Figure 5. (b) Data extracted from the two sharp peaks in Figure 5a at around 440 and 570 cm^{-1}. (c) Data corresponding to the strongest peak in Figure 5b at 830 cm^{-1}. In parts a and b, filled marks correspond to the data obtained from the lower frequency peak, and open marks correspond to the data obtained from the higher frequency peak. Broken lines are guides for the eyes.

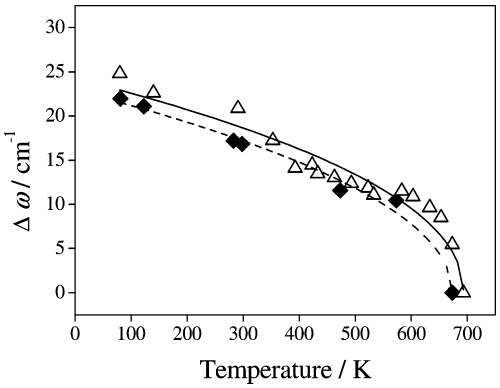

Figure 8. Temperature dependence of the difference between the two peaks shown in Figure 6 at around 138 cm^{-1}. Data collected from the two different samples sintered at 1273 K for 24 h and 1073 K for 12 h are indicated by open triangles and filled diamonds, respectively. It was estimated that SMW transforms to the cubic phase at around 693 K for the former case and 673 K for the latter case.

temperature reached the transition point around 693 K. One explanation for this could be that the phase transition to the cubic phase occurs via an intermediate phase (for instance, via a phase whose symmetry group is a subgroup of the $Fm\bar{3}m$ space group and a supergroup of the $P4_2/n$ space group). This would be consistent with the observation in ref 17.

5. Conclusions

Temperature and wavelength dependencies of the Raman spectra measured from single phase BMW and SMW samples, prepared through the PC method, were investigated. The main goals were to study the symmetries versus temperature, to study the ordering of Mn and W ions over the B-cation sites, and to determine the role of Mn ions in the lattice dynamics through resonance Raman scattering.

Raman spectra of the BMW sample did not significantly change in the temperature range between 80 and 900 K and were consistent with cubic symmetry (space group $Fm\bar{3}m$). Particular attention was paid to the line broadening of the BMW sample. It was found that the frequency and temperature dependent line broadening of the two pure oxygen modes correspond to the normal anharmonic interactions between phonons. On the contrary, the line widths of the two T_{2g} modes were very narrow and almost constant against temperature change. Thus, no evidence for compositional disorder at the B-cation site was found. A broad band, consisting of numerous peaks, was observed between 450 and 750 cm^{-1}. The intensity of this band was increasing with increasing laser light wavelength. The origin of these peaks was assigned to the Franck−Condon modes, related to the electronic transitions in Mn ions. In contrast to the previous studies, we found the role of Mn ions for the lattice dynamics of these double perovskites to be important.

SMW has a tetragonal phase that is slightly distorted from the ideal cubic double perovskite structure (such as was found for the BMW sample). Raman scattering results showed that this distortion continuously decreased with increasing temperature, and finally, a phase transition to the cubic phase occurred at around 670 K (for the sample sintered at 1073 K) or at around 690 K (for the sample sintered at 1273 K). The difference in phase transition temperatures was related to the differences in the average crystal size. As some Raman peaks in the low-frequency region vanished before the transition temperature, it might be that the phase transition occurs via an intermediate phase.

Acknowledgment. We are grateful to Professors E. Yasuda and M. Yoshimura for supporting this study. We would also like to thank Drs. S. Eriksson, A. K. Azad, and M. Osada for their valuable discussions. Y.F. is grateful to the Japan Society for the Promotion of Science and the Academy of Finland (AF) for their financial support. J.F. wishes to thank the AF (Project Nos. 207071 and 207501) for financial support.

References and Notes

(1) Jaffe, B.; Cook, W. R.; Jaffe, H. *Piezoelectric Ceramics*; Academic Press: London, 1971.

(2) Pauling, L. *J. Am. Chem. Soc.* **1924**, *46*, 2738.
(3) Kobayashi, K.-T.; Kimura, T.; Sawada, H.; Terakura, K.; Tokura, Y. *Nature* **1998**, *395*, 677.
(4) *CRC Handbook of Chemistry and Physics*, 80th ed.; CRC Press: Boca Raton, FL, 1999.
(5) Kakihana, M. *J. Sol-Gel Sci. Technol.* **1996**, *6*, 7.
(6) Fujioka, Y.; Kakihana, M. *Trans. Mater. Res. Soc. Jpn.* **2003**, *28*, 373.
(7) Fujioka, Y.; Frantti, J.; Eriksson, S.; Azad, A. K.; Kakihana, M. *NFL annual report*; Uppsala University: Nyköping, Sweden, 2003. A copy is available upon request.
(8) Khattak, C. P.; Cox, D. E.; Wang, F. F. Y. *J. Solid State Chem.* **1976**, *7*, 323.
(9) Azad, A. K.; Ivanov, S.; Eriksson, S.-G.; Eriksen, J.; Rundlöf, H.; Mathieu, R.; Svedlindh, P. *Mater. Res. Bull.* **2001**, *36*, 2215.
(10) Azad, A. K.; Ivanov, S.; Eriksson, S.-G.; Rundlöf, H.; Eriksen, J.; Mathieu, R.; Svedlindh, P. *J. Magn. Magn. Mater.* **2001**, *237*, 124.
(11) Liegeois-Duychaerts, M.; Tarte, P. *Spectrochim. Acta* **1974**, *30A*, 1711.
(12) Fujioka, Y.; Frantti, J.; Kakihana, M. *J. Phys. Chem. B* **2004**, *108*, 17012. Single X-ray diffraction measurements confirmed the Raman results according to which the symmetry of this single crystal was cubic. The crystal symmetry is affected by crystal size, stoichiometry, and strains within grain boundaries (in the case of powder), which are possible reasons for the observed symmetry differences.
(13) Dove, M. T. *Introduction to Lattice Dynamics*; Cambridge University Press: Cambridge, 1993.
(14) Ritter, C.; Ibarra, M. R.; De Teresa, J. M.; Algarabel, P. A.; Marquina, C.; Blasco, J.; Garcia, J.; Oseroff, S.; Cheong, S-W. *Phys. Rev. B* **1997**, *56*, 8902.
(15) Zhang, N.; Yang, W.; Ding, W.; Xing, D.; Du, Y. *Solid State Commun.* **1999**, *109*, 537.
(16) Sanchez, R. D.; Rivas, J.; Causa, M. T.; Tovar, M.; Oseroff, S. *Appl. Phys. Lett.* **1996**, *68*, 134.
(17) Azad, A. K.; Eriksson, S.-G. *Solid State Commun.* **2003**, *126*, 503.